PHILOSOPHICAL TRANSACTIONS A

rsta.royalsocietypublishing.org

Research

Article submitted to journal

Subject Areas:
Tidal energy, hydrodynamics, optimisation

Keywords:
Economics, Alderney Race, Tidal Stream Energy, Array Optimisation, Levilised Cost Of Energy

Author for correspondence:
Z. L. Goss
e-mail: z.goss15@imperial.ac.uk

Identifying economically viable tidal sites within the Alderney Race through optimisation of LCOE

Z. L. Goss[1], D. S. Coles[2,3] and M. D. Piggott[1]

[1]Department of Earth Science and Engineering, Imperial College London, SW7 2AZ, UK
[2]Energy and Climate Change Division, Sustainable Energy Research Group, School of Engineering, University of Southampton, Southampton, SO16 7QF, UK
[3]SIMEC Atlantis Energy, 4th Floor, Edinburgh Quay 2, 139 Fountainbridge, Edinburgh EH3 9QG, UK

Costs of tidal stream energy generation are anticipated to fall considerably with array expansion and time. This is due to both economies of volume, where arrays comprising of large numbers of turbines can split fixed costs over a greater number of devices, and learning rates, where the industry matures and so arrays of the same size become cheaper through the lessons learnt from previous installations. This paper investigates how tidal energy arrays can be designed to minimise the levelised cost of energy (LCOE), by optimising not only the location but also the number of devices, to find a suitable balance between decreased costs due to economies of volume and diminishing returns due to global blockage effects. It focuses on the Alderney Race as a case study site due to the high velocities found there, making it a highly suitable site for large scale arrays. It is demonstrated that between 1 and 2 GW could be feasibly extracted as costs in the tidal industry fall, with the LCOE depending greatly on the assumed costs. A Monte-Carlo analysis is undertaken to account for variability in capital and operational cost data used as inputs to the array optimisation. Once optimised, the estimated P50 LCOE of an 80 MW array is £110/MWh. This estimate aligns closely with the level of subsidy considered for tidal stream projects in the Alderney Race in the past.

THE ROYAL SOCIETY PUBLISHING

The Alderney Race contains a significant tidal energy resource, with a maximum average power potential of 5.1 GW and large regions of the Race exhibiting velocities of up to 5 m/s [1]. In order to develop tidal stream energy projects in the Alderney Race, there is a need to understand how the resource can be harnessed most cost effectively. Through phased array development, the cost of energy can be reduced as the industry matures and array deployments within the Alderney Race expand.

Newly developed methods for optimising the placement of tidal stream turbines within arrays have demonstrated potential to increase array efficiency (energy yield per turbine) by up to 100% in some cases, thereby providing an avenue for further cost of energy reduction [2]. This gradient-based optimisation approach is implemented within a full hydrodynamics solver in order to link the changes to the hydrodynamics caused by the iterative movement of turbines within the optimisation to the resulting power of the array. This is a critical requirement when optimising large arrays in order to account for array scale blockage, as has been demonstrated in [3].

In this paper, we implement array optimisation in the Alderney Race to minimise the Levelised Cost of Energy (LCOE). We implement a proxy for learning rates and economies of volume based on information in the literature in order to propose optimal phased array development in the Alderney Race, where these cost reductions unlock ongoing array development. The array optimisation is implemented within the *Thetis* hydrodynamic model, which is described in Section 2. The model is validated using four bed mounted ADCP datasets and tidal gauge data from around the model domain (Section 3). The optimisation approach is described in Section 4(a). Results from the optimisation are presented and discussed in Section 4(b).

2. Hydrodynamic model

The nonlinear shallow water equations are discretised using the finite element method, via the flexible coastal ocean modelling software *Thetis* [4,5], implemented within the *Firedrake* [6] finite element code generation framework. The $\mathrm{P_{1DG}} - \mathrm{P_{1DG}}$ velocity-pressure finite element pair is used for spatial discretisation. The semi-implicit Crank-Nicolson time stepping method is used for temporal discretisation, with a constant time step of $\Delta t = 600s$. These discretisation options are second order accurate in space and time, as verified for the three-dimensional version of the *Thetis* model in [7] and for the two-dimensional depth-averaged version (which is the one used in this work) in [8]. The model domain, which covers the majority of the English Channel, is shown in Figure 1. The model is forced by Q1, O1, P1, K1, M2, S2, N2, K2 and M4 constituent elevation forcing at the open boundaries, implemented via the *Uptide*[1] package using data extracted from the OSU Tidal Prediction Software (OTPS) [9]. *Thetis* solves the non-conservative form of the nonlinear shallow water equations;

$$\frac{\partial \eta}{\partial t} + \nabla \cdot (H\mathbf{u}) = 0, \tag{2.1}$$

$$\frac{\partial \mathbf{u}}{\partial t} + \mathbf{u} \cdot \nabla \mathbf{u} - \nu \nabla^2 \mathbf{u} + f\mathbf{u}^{\perp} + g\nabla\eta = -\frac{\tau_b}{\rho H}, \tag{2.2}$$

where η is the free surface perturbation, t is time, H is the total water depth, $f\mathbf{u}^{\perp}$ is the Coriolis forcing described by Equation (2.4), where $\mathbf{u}^{\perp}$ is the velocity vector rotated counter-clockwise 90^o, $\mathbf{u} = (u, v)$ is the depth-averaged velocity vector, ν is the kinematic viscosity of the fluid, g is acceleration due to gravity, τ_b is the bed friction and ρ is the water density. Over the majority of the domain the kinematic viscosity is set to a value of 10 $\mathrm{m^2 s^{-1}}$. This artificially increased value acts primarily as a stabilisation mechanism and accounts for scales of motion not resolved at the mesh resolutions utilised. At the open boundaries, the viscosity is increased to a value of 1000 $\mathrm{m^2 s^{-1}}$, over a region extending 50km from the open boundaries. This acts as a further stabilisation mechanism for any spurious flow behaviour that can be generated through minor inconsistencies

[1] https://github.com/stephankramer/uptide

(e.g. due to different resolution and bathymetry data employed) between our model and set-up, and the configuration used to generate the tidal harmonic forcing data. This has negligible impact on the flow speeds within areas of interest for energy extraction. The location of the open boundaries are also chosen, in part, to be far enough away from the array location such that changes in hydrodynamics do not propagate significantly back to the open boundaries, which would invalidate the assumption of unchanged boundary forcing. Justification of the selection of the time step and kinematic viscosity described above, is given through a sensitivity test in Section 3(b)i.

The bottom friction, τ_b, is calculated using the Manning formulation;

$$\frac{\tau_b}{\rho} = gn^2 \frac{||\mathbf{u}||\mathbf{u}}{H^{\frac{1}{3}}}, \tag{2.3}$$

where n is the Manning coefficient, which is uniformly applied over the whole domain and tuned during model calibration in Section 3(b)iii.

The Coriolis forcing, $f\mathbf{u}^{\perp}$, is represented by the beta-plane approximation, due to the size of the domain, such that;

$$f = f_0 + \beta y, \tag{2.4}$$

where the Coriolis and Rossby parameters are given by;

$$f_0 = 2\Omega \sin(\zeta), \qquad \beta = \frac{1}{R} 2\Omega \cos(\zeta), \tag{2.5}$$

respectively, where Ω is the angular frequency of the Earth's rotation, ζ the latitude and R is the earth's radius.

Additional meteorological forcings such as wind and atmospheric pressure have not been included here. Some studies have found that the effects of wind-driven waves can have a notable impact on the tidal power extraction, especially in extreme and winter conditions [10,11]. However, tide-induced currents are the dominant forcing for tidal current estimation, especially at the depths concerned for tidal energy extraction [12]. For this reason, the exclusion of these additional meteorological forcings is common in regional scale hydrodynamic modelling work, such as [1,13–15].

Bathymetry data was obtained from the Marine Digimap database [17], with 1 arc-second resolution ($\approx$ 30 m) over the Northern half of the Channel and 6 arc-second resolution ($\approx$ 180 m) over the Southern half of the Channel. There is a small region around Normandy that is not covered by the Marine Digimap database. For this region bathymetry was obtained from the General Bathymetric Chart of the Oceans (GEBCO) 2014 dataset with 30 arc-second resolution ($\approx$ 900 m) [18].

Coastlines were adapted from the Global Self-consistent, Hierarchical, High-resolution Geography Database (GSHHG) [19]. Coastline geometry has been simplified to remove estuaries and islands (except for the islands closest to Alderney). This was done to reduce computational expense as it enables lower mesh resolution to be used around the coastlines of the domain while having minimal impact on the region of interest [20].

The model employs an unstructured triangular mesh, allowing variable mesh resolution across the domain, as shown in Figure 1. A mesh independence study was carried out to establish the most suitable mesh resolution to achieve accurate ambient flow results at acceptable computational expense. Table 1 summarises the resolution and number of nodes/elements in the four meshes considered in the mesh independence study. Results from the mesh independence study are presented in Section 3(b)ii, demonstrating that mesh independence was achieved with Mesh 3. Mesh 3 has a resolution of 500 m within the tidal energy plots in the Alderney Race, 2,000 m around coastlines and 10,000 m within the rest of the domain. The mesh comprises of 14,260 unstructured triangular elements and 7,126 nodes.

3. Calibration and Validation

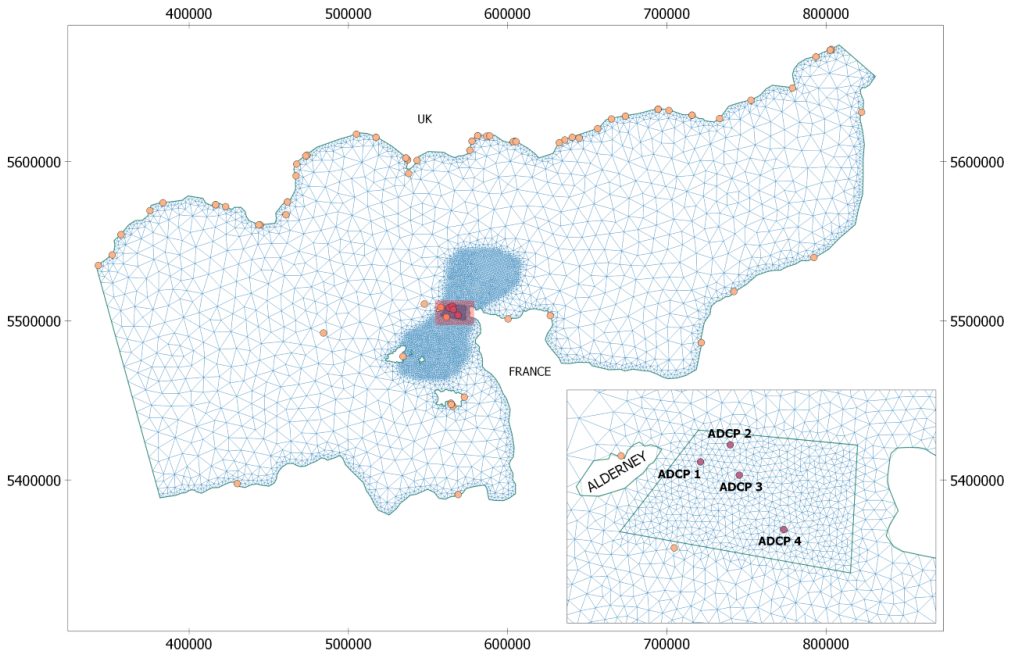

Figure 1: The unstructured triangular mesh used in the shallow water English Channel model, with the locations of the four ADCPs (purple pointers) and the 68 tide gauges (yellow pointers) used to validate the model [16]. The farm area considered is also shown within the Alderney Race.

Table 1: Resolution and node/element count of meshes used in the mesh independence study.

	Tidal Plot	Alderney Race	Shorelines	Rest of domain	Nodes	Elements
Mesh 1	1000m	2000m	4000m	10000m	2876	5760
Mesh 2	750m	1500m	3000m	10000m	4086	8180
Mesh 3	500m	1000m	2000m	10000m	7126	14260
Mesh 4	375m	750m	1500m	10000m	11485	22978

(a) Methods

The *Thetis* model was calibrated by varying the bed drag to establish the value of Manning coefficient that achieves the highest level of agreement with field measurements of flow speed and tidal elevation. In similar tidal calibration studies (e.g. [21]) non-dimensional quadratic drag coefficients, c_D, typically in the range 0.0025 to 0.0075 have been considered. The quadratic drag coefficient can be converted to a Manning coefficient using [22];

$$c_D = g n^2 h^{-1/3}, \tag{3.1}$$

where g is acceleration due to gravity, n is the Manning coefficient and $h = 35m$ is the representative depth in the Alderney Race. This results in a Manning coefficient range of approximately 0.03 to 0.05 $sm^{-1/3}$. In this study five values of Manning coefficient were considered: 0.02, 0.025, 0.03, 0.035 and 0.04 $sm^{-1/3}$. Section 3(a) provides a description of the methods used to carry out the model calibration and validation. Results from the calibration and validation studies are presented in Sections 3(b) and 3(c).

(i) Flow speeds

An industry partner provided data from three bed mounted ADCP campaigns within the Alderney Race, which were used to calibrate the model. The ADCP datasets provide 10 minute averages of flow speed and direction within 1 m vertical bins spanning the majority of the water column. The datasets cover a 1 month period. The flow speed and directions obtained from the ADCPs were depth averaged to compare against simulated results.

Five separate simulations were run using the aforementioned Manning coefficients. The model accuracy was quantified using three different metrics. The Normalised Root Mean Squared Error (NRMSE) provides a comparison between simulated and measured flow speeds;

$$NRMSE = \frac{1}{\max(mes_i)} \sqrt{\frac{1}{N} \sum_{i=1}^{i=N} (mod_i - mes_i)^2} \tag{3.2}$$

where mes_i is the measured data obtained from the bed mounted ADCPs at time step i and mod_i is the model prediction at time step i.

The Index of Agreement (IA), also known as the Willmott Index [23], is used as a relative covariability of the model predictions and ADCP observations about an estimate of the 'true' mean. Bias (B) and Relative Bias (RB) are also used to quantify the systematic error of the model in simulating the flow. This is consistent with the approach taken in [24] and [25]. These quantities are defined mathematically as;

$$IA = 1 - \frac{\sum_{i=1}^{i=N} (mod_i - mes_i)^2}{\sum_{i=1}^{i=N} (|mod_i - \bar{mes_i}| + |mes_i - \bar{mes_i}|)^2}, \tag{3.3}$$

$$B = \bar{mod_i} - \bar{mes_i}, \qquad RB = 100 \frac{B}{\bar{mes_i}}, \tag{3.4}$$

The model was validated against an additional sea bed mounted ADCP dataset (ADCP 4) obtained in the Alderney Race [26]. This dataset covered a period of 14.6 days, providing flow speeds and directions at hourly intervals. The location of the four ADCP deployments in the Alderney Race are shown in Figure 1.

(ii) Tidal elevations

Free surface elevation data was extracted from 68 locations around the domain to compare against tide gauge data. The tide gauge locations are shown in Figure 1 [16]. For each of the Manning coefficients used to tune the model, the *Thetis* simulation was run over a two month period and the elevation predictions at each of the tide gauge and ADCP locations were extracted. Least squared regression was performed on the η time signal, via the *Uptide* python package, to calculate the model phase and amplitude for each of the harmonic constituents in the tidal forcing. These were then compared either directly to the tide gauge phase and amplitude readings or to phase and amplitudes calculated in the same manner from elevation time series readings at the location of each of the ADCPs. The model amplitude error, $100 \cdot (amp_{mod} - amp_{mes})/amp_{mes}$, and phase error, $(pha_{mod} - pha_{mes})^\circ$, for the two most dominant constituents in the region, M2 and S2, are presented below.

The time period of the signal must be long enough to distinguish each pair of constituents, and this required period can be calculated in *Uptide* using the Rayleigh Criterion. Most pairs can be resolved within a month, however S2 & K2 and P1 & K1 require much longer to resolve, and so, for the purpose of harmonic validation, the latter of each pair (the constituent which is smaller in magnitude in the region) was removed. All nine constituents were included in models for all other purposes except harmonic validation.

(b) Calibration results

(i) Model stability

The impact of varying both the kinematic viscosity and time step were investigated using a Manning coefficient value of $0.03sm^{-1/3}$. Increasing the time step through $\Delta t = 30, 60, 300, 600, 1200$ seconds resulted in a velocity magnitude NRMSE for ADCPs 1–3 of 11.7%, 11.5%, 11.8%, 11.8% and 12.5%, respectively. A time step of 600 seconds was selected for future runs since (a) it was computationally prohibitive to use a smaller time step within the adjoint optimisation loop, and (b) only minor changes in model results where exhibited for the time step range considered when compared to ADCP data.

ADCP 4 was used to test the sensitivity of the model to changes in the kinematic viscosity, using $\nu = 1, 10, 100, 1000$ m^2s^{-1}. The $\nu = 1$ m^2s^{-1} case resulted in model instability. The remaining kinematic viscosity cases resulted in a velocity magnitude NRMSE of 10.2 %, 10.8 % and 12.3 %, respectively. A viscosity of $\nu = 10$ m^2s^{-1} was selected since it provided the lowest NRMSE in velocity whilst also providing model stability.

(ii) Mesh sensitivity

Figure 2a compares the flow speed time series obtained from model simulations (using Meshes 1-4) and the ADCP measurements. The difference in peak flow speeds obtained by Meshes 1 and 2 is approximately 0.2 m/s. Further refinement of the mesh reduces the difference in peak flow speeds (obtained by Mesh 3 and 4) to 0.1 m/s.

Table 2 shows the NRMSE for each combination of mesh and Manning coefficient tested. There was on average a 0.66% improvement in NRMSE between Meshes 3 and 4 across the range of Manning coefficients tested. Mesh 1 took under 2 hours to model 60 days, Mesh 2 took under 4 hours, Mesh 3 took just over 5 hours and Mesh 4 took just over 11 hours. This is a significant increase in the computational expense for a relatively small difference between models. The computational expense for a single model run is of key importance as the array optimisation aspect of the modelling is fully coupled to the hydrodynamics – for every iteration of the optimisation algorithm, the forward model needs to be re-run to calculate the updated hydrodynamics. Therefore Mesh 3 was chosen for the following work.

Table 2: The *Thetis* model NRMSE, averaged over ADCP's 1–3

	Manning coefficient ($sm^{-1/3}$)				
	0.02	0.025	0.03	0.035	0.04
Mesh 1	13.7 %	11.8 %	12.6 %	15.2 %	18.6 %
Mesh 2	13.7 %	11.8 %	12.3 %	14.9 %	18.5 %
Mesh 3	13.5 %	11.2 %	11.8 %	14.2 %	17.7 %
Mesh 4	14.5 %	11.0 %	10.4 %	12.9 %	16.3 %

(iii) Calibration – flow speed

Figures 2b–2d compare the flow speed time series obtained using Mesh 3 for each of the Manning coefficients considered. These results are compared against field data obtained from the ADCPs. To protect the confidential nature of the ADCP data we do not specify a start date and instead show time in days from the start of the model. The time series data demonstrates that the flow speeds are relatively sensitive to the Manning coefficient, as there is approximately a 0.5 m/s difference in peak flow speeds across the range of Manning coefficients used.

Table 3 provides the error metrics achieved for each of the Manning coefficients considered at each ADCP location. Closest agreement between simulated and measured NRMSE velocities was achieved using a Manning coefficient of $0.025sm^{-1/3}$ and $0.03sm^{-1/3}$, depending on location within the Alderney Race. Closest agreement with ADCP 1 and 2 was achieved using

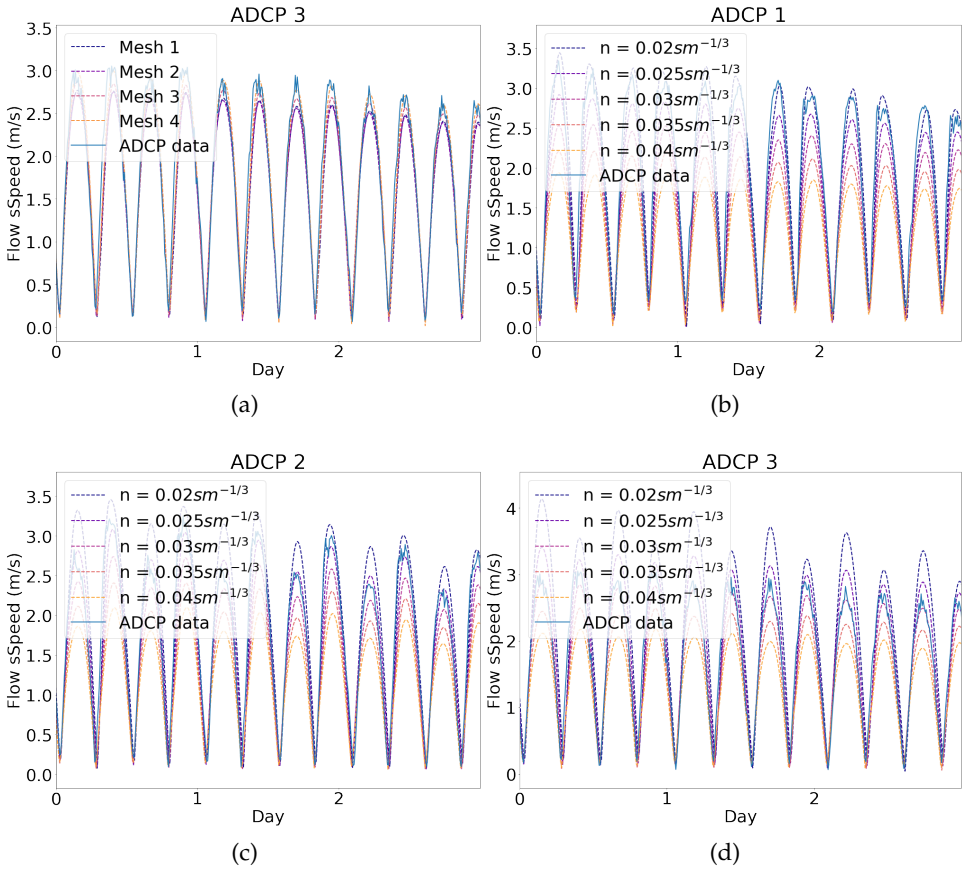

Figure 2: The sensitivity of the *Thetis* model velocity magnitude predictions to (a) changes in the mesh resolution for a Manning coefficient of $0.03sm^{-1/3}$, at ADCP 3, and to changes in the Manning coefficient, at (b) ADCP 1, (c) ADCP 2 and (d) ADCP 3, all while using Mesh 3.

$n = 0.025sm^{-1/3}$, resulting in an average NRMSE across the three ADCPs of 12.4 and 9.7%) respectively. Reasonable agreement was also achieved using $n = 0.03sm^{-1/3}$, which achieved an NRMSE of 15% and 11% respectively). Closest agreement with ADCP 3 was achieved with $n = 0.03sm^{-1/3}$ (9.4%), with $n = 0.035sm^{-1/3}$ (11.1%) and $n = 0.025sm^{-1/3}$ (11.6%) also having close levels of performance. The biases show that for Manning coefficients of $0.03sm^{-1/3}$ and above, the model underestimates the flow speeds at all ADCP locations. For a Manning coefficient of $n = 0.02sm^{-1/3}$, flow velocities at ADCP 3 are overestimated. For a Manning coefficient of $n = 0.025sm^{-1/3}$, flow velocities at ADCP's 2 and 3 are overestimated.

(iv) Calibration – free surface elevation

Table 4 provides a comparison of modelled vs. actual M2 and S2 elevation amplitudes and phases at the ADCP locations. Closest agreement was achieved using a Manning coefficient of 0.03 $sm^{-1/3}$, where M2 and S2 phase were predicted very well (0.1–1.0° and 0.5–2.1° error respectively) and the M2 and S2 amplitudes had errors ranging between 9.7–17.7% and 1.3–10.2% respectively.

Table 5 shows the M2 and S2 elevation amplitude errors from the *Thetis* model relative to the tide gauge readings. Closest agreement was achieved for $n = 0.025sm^{-1/3}$. However, $n = 0.03sm^{-1/3}$ achieved very similar performance. For a Manning coefficient of $0.03sm^{-1/3}$, the M2 and S2 normalised phase errors were 16.7% and 16.4% respectively, whereas for a Manning

Table 3: The *Thetis* velocity amplitude model error metrics at ADCPs 1–3 for different Manning coefficients.

	Manning coefficient ($sm^{-1/3}$)				
	0.02	0.025	0.03	0.035	0.04
NRMSE 1	11.7 %	12.4 %	15.0 %	18.4 %	21.9 %
NRMSE 2	11.4 %	9.7 %	11.0 %	13.2 %	16.4 %
NRMSE 3	17.4 %	11.6 %	9.4 %	11.1 %	14.7 %
NRMSE (Avg)	13.5 %	11.2 %	11.8 %	14.2 %	17.7 %
IA 1	0.938	0.926	0.885	0.826	0.762
IA 2	0.944	0.954	0.936	0.902	0.843
IA 3	0.895	0.946	0.960	0.938	0.884
IA (Avg)	0.925	0.942	0.927	0.889	0.830
Bias 1 (m/s)	-0.06	-0.22	-0.36	-0.50	-0.62
Bias 2 (m/s)	0.10	-0.06	-0.21	-0.32	-0.44
Bias 3 (m/s)	0.27	0.09	-0.08	-0.24	-0.38
Relative Bias 1	-3.4 %	-12.7 %	-21.3 %	-29.2 %	-36.4 %
Relative Bias 2	6.1 %	-3.6 %	-13.2 %	-20.9 %	-28.5 %
Relative Bias 3	16.6 %	5.7 %	-5.1 %	-14.8 %	-23.6 %

Table 4: The *Thetis* model prediction and error in the M2 and S2 phase and amplitude, for each Manning coefficients tested. Harmonic analysis is performed on η readings taken at the locations of ADCPs 1–3.

	Manning coefficient ($sm^{-1/3}$)				
ADCP	0.02	0.025	0.03	0.035	0.04
			M2 Amplitude		
1	1.82 (-13.3%)	1.86 (-11.3%)	1.90 (-9.7%)	1.90 (-9.3%)	1.90 (-9.6%)
2	1.78 (-14.0%)	1.82 (-11.9%)	1.85 (-10.5%)	1.86 (-10.0%)	1.86 (-10.2%)
3	1.90 (-20.0%)	1.94 (-18.5%)	1.96 (-17.7%)	1.96 (-17.5%)	1.96 (-17.9%)
			S2 Amplitude		
1	0.75 (-3.9%)	0.76 (-3.3%)	0.76 (-3.3%)	0.75 (-4.3%)	0.74 (-5.9%)
2	0.74 (-2.0%)	0.74 (-1.2%)	0.74 (-1.3%)	0.74 (-2.2%)	0.72 (-3.7%)
3	0.79 (-9.5%)	0.79 (-9.5%)	0.78 (-10.2%)	0.77 (-11.4%)	0.76 (-13.1%)
			M2 Phase		
1	197.23 ° (-1.2 °)	198.52 ° (0.1 °)	199.38 ° (1.0 °)	199.78 ° (1.4 °)	200.01 ° (1.6 °)
2	198.79 ° (-1.8 °)	199.98 ° (-0.6 °)	200.74 ° (0.1 °)	201.01 ° (0.4 °)	201.14 ° (0.5 °)
3	198.58 ° (-0.6 °)	199.56 ° (0.4 °)	200.20 ° (1.0 °)	200.47 ° (1.3 °)	200.62 ° (1.5 °)
			S2 Phase		
1	254.47 ° (-3.7 °)	256.41 ° (-1.7 °)	257.60 ° (-0.5 °)	258.27 ° (0.1 °)	258.82 ° (0.7 °)
2	255.87 ° (-5.1 °)	257.70 ° (-3.2 °)	258.81 ° (-2.1 °)	259.34 ° (-1.6 °)	259.80 ° (-1.1 °)
3	255.75 ° (-3.5 °)	257.32 ° (-1.9 °)	258.30 ° (-0.9 °)	258.84 ° (-0.4 °)	259.33 ° (0.1 °)

Coefficient of $0.025sm^{-1/3}$, they were 13.8% and 13.4%, respectively. This suggests that further work could use a variable bed friction throughout the channel, based on maps of bed type such as the "Service Hydrographique et Océanographique de la Marine Service" (SHOM) [27], as used in [24], since a coefficient of $0.03sm^{-1/3}$ generally produced better results for ADCPs and gauges within the Race, whilst a coefficient of $0.025sm^{-1/3}$ produced better results for tide gauges spread throughout the wider Channel.

Inspection of the ADCP 1–3 velocity time series data against the *Thetis* model and harmonic analysis of the M2 and S2 elevation phase and amplitude have shown that closest agreement

Table 5: The *Thetis* model M2 and S2 amplitude errors over the 68 tide gauge locations.

	Manning coefficient ($sm^{-1/3}$)				
Error type	0.02	0.025	0.03	0.035	0.04
M2 RMSE	0.219 m	0.233 m	0.281 m	0.347 m	0.416 m
M2 NRMSE	13.0 %	13.8 %	16.7 %	20.6 %	24.7 %
S2 RMSE	0.081 m	0.078 m	0.096 m	0.123 m	0.152 m
S2 NRMSE	13.8 %	13.4 %	16.4 %	21.2 %	26.1 %

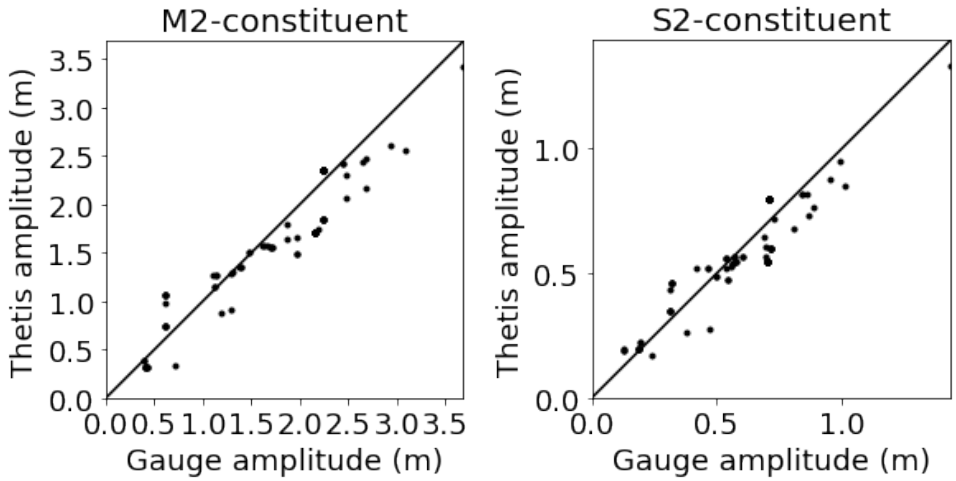

Figure 3: The M2 and S2 amplitude of the 68 tide gauges across the English Channel against the *Thetis* model predictions, for a Manning coefficient of $n = 0.03sm^{-1/3}$.

was achieved with a Manning coefficient $0.03sm^{-1/3}$. The NRMSE of ADCP 1–3 velocity time series data and the harmonic analysis of the elevation at the 68 tide gauges showed slightly better results for $0.025sm^{-1/3}$ (11.2% v.s. 11.8%). On balance, for this work a Manning coefficient of $0.03sm^{-1/3}$, applied uniformly over the domain, was established as the most suitable value to take forward to the array optimisation study.

(c) Validation

The model was calibrated with ADCPs 1–3, leaving ADCP 4 from [26] for independent validation. Table 6 provides a comparison of the NRMSE, Bias, Relative Bias and Index of Agreement at the location of ADCP 4, obtained from the five bed drag coefficient cases.

The NRMSE and Index of Agreement results suggest that the $n = 0.03sm^{-1/3}$ case provides best agreement with ADCP 4 data, reinforcing the choice of the Manning coefficient from the calibration tests. However, the difference between these results and those obtained with $n = 0.025sm^{-1/3}$ is small and the bias is lowest at $n = 0.025sm^{-1/3}$. For comparison, the RMSE at ADCP 4 with $n = 0.03sm^{-1/3}$ is 0.243 m/s, whereas [24] achieved a RMSE of 0.15–0.26 m/s, a relative bias of between -1% and -8%, and an IA of 0.962–0.990 using a model with 100 m resolution and a time step of 10 seconds.

4. Economic resource assessment

Table 6: The *Thetis* velocity amplitude model error at ADCP 4 for different Manning coefficients.

	Manning coefficient ($sm^{-1/3}$)				
	0.02	0.025	0.03	0.035	0.04
NRMSE	21.8 %	11.3 %	10.2 %	15.7 %	21.5 %
Bias (m/s)	0.19	-0.01	-0.16	-0.31	-0.44
Relative Bias	13.8 %	-0.6 %	-11.7 %	-22.9 %	-32.3 %
IA	0.859	0.956	0.960	0.898	0.809

(a) Method

Turbines were introduced into the *Thetis* model via the inclusion of a turbine drag coefficient, c_t, which appears within an additional sink term in the momentum equation of the form;

$$\frac{c_t}{\rho H}||\mathbf{u}||\mathbf{u}. \tag{4.1}$$

The additional turbine drag coefficient is added to the existing sea-bed drag coefficient at the location of the turbines. The added turbine drag coefficient is applied continuously over the array area, and is allowed to vary spatially depending on the local density of turbines. This continuous approach for parameterising array drag was favoured over the more computationally expensive discrete approach, where each individual turbine is allocated its own drag term [28]. The discrete approach requires a mesh with element sizes constrained to be below the turbine rotor diameter to allow individual turbines to be resolved. The continuous approach is particularly well suited to the problem at hand because it allows for the number of turbines as well as their positions to be simultaneously optimised for. In [2] flow modelling from the continuous and discrete turbine representations are compared, showing that the farm wake and bypass flow modelled by both methods are largely consistent. However, the continuous method does not resolve the individual wakes within the farm area. Inter-array flow effects such as the impingement of wakes on downstream turbines are mitigated to an extent in this work by constraining the minimum longitudinal spacing between turbines to ten rotor diameters. This turbine spacing constraint is informed by guidelines published by the European Marine Energy Centre (EMEC) [29]. In taking this approach, this work provides a valid approach to modelling large scale arrays in order to model the impacts of array scale blockage on energy yield.

The turbine drag coefficient c_t can be found from a spatially varying turbine density field, $d(x)$, via the relationship;

$$c_t(d(x)) = \frac{1}{2}\, C_T\, A_T\, d(x), \tag{4.2}$$

where C_T is the thrust coefficient, A_T is the swept area of a turbine, and $d(x)$ corresponds to the number of turbines per metre squared of seabed [2].

The swept area and rated power of the turbines used in this work are assumed to be 16 m and 2 MW respectively. This is informed by (a) the scale of turbines in operation currently and (b) the depths within the Alderney Race. Typically, turbines in operation at present have rotor diameters and rated capacity ranging between 9 m – 18 m and 100 kW – 1.5 M respectively, e.g. such as the Nova Innovation turbines at the Shetland Tidal Array [30] and the SIMEC Atlantis Energy and Andritz Hydro Hammerfest turbines at the MeyGen array [31]. Studies suggest that increasing the rotor diameter and rated power can be key drivers for reducing the cost of tidal stream energy in the future [32], and SIMEC Atlantis Energy have developed a 2 MW turbine with 20–24m rotors for the next phase of the MeyGen project [33]. However, the rotor diameter of the turbines are limited here in regions of the East Race since it is relatively shallow. On balance, 16 m diameter 2 MW turbines were chosen to be representative of future commercial turbines that may be deployed in this region. It is acknowledged that in reality, a variety of turbine sizes are needed given the spatial variation in depth across the Race, as demonstrated in [3], and this is an area identified for further work.

Below the rated speed the thrust and power coefficient are assumed equal to $C_T = 0.8$ [34] and $C_P = 0.41$ [31] respectively. Above rated speed, the coefficients are scaled by $\frac{u_{rated}^3}{u^3}$ to maintain constant drag and power. The turbine density is set to zero outside of the array area, Ω, shown in Figure 1, and within the array it is allowed to vary continuously up to a density value which corresponds to a spacing of 2.25 diameters laterally (centre-to-centre) and 10 diameters longitudinally [29].

To optimise the array, a gradient-based optimisation algorithm is employed which utilises *Thetis*'s adjoint to obtain the required gradient, where c_t is the control parameter for evaluating the sensitivity of the optimisation functional, and is the quantity that is updated at every optimisation iteration. Further details may be found in [2]. The array design, including the number of turbines (obtained via the integral of the turbine density field) and their spatial distribution, is optimised with respect to a functional J which here takes the form;

$$J = P_{\text{avg}} - P_{\text{BE}} \times n_t. \tag{4.3}$$

where P_{avg} is the average power generated by the whole array and n_t is the number of turbines in the array. P_{BE} is the break even power, which is the time-averaged power that a turbine must generate to be economically viable for the project. In this work the break even power is varied between 0 to 700 kW. A 2 MW turbine that achieves a time averaged power of 700 kW is performing with a capacity factor of 35%. An increase in break even power results in a decrease in the optimal number of turbines in the array. In this case adding additional turbines has a detrimental impact on the power generated per turbine, because the added turbines increase array blockage, slowing the flow velocities and hence reducing the available power to the array, so that the break even power cannot be achieved. This is overcome within the optimisation by reducing the number of turbines in the array.

The power generated by the array is calculated at each time step by integrating over the farm area, Ω, via the approximation

$$P = \frac{1}{2}\rho A_T \int_\Omega C_P \, d(x) \, ||\mathbf{u}||^3 \, dx. \tag{4.4}$$

The power can be time averaged and combined with the number of turbines, n_t, in the array design at that iteration, which can be obtained from c_t via

$$\int_\Omega c_t(d(x)) \, dx = \frac{1}{2} C_T A_T n_t. \tag{4.5}$$

The optimisation was run over a representative 14.5 day spring-neap cycle, ensuring a sufficient duration to capture the dominant tidal variations whilst also achieving acceptable computational time for the optimisation to converge. The model was spun up for one day before each optimisation iteration.

Once the optimisation completed for each of the break even powers considered, the Levelised Cost Of Energy (LCOE) of each optimal array was calculated. The Levelised Cost of Energy (LCOE) describes the fixed price per MWh that needs to be received by the developer for an array to break even over its lifetime. It is calculated using;

$$\text{LCOE} = \frac{\text{CA}_f + \text{CA}_t \times n_t + \sum_{i=1}^{L} \frac{\text{O}_f + \text{O}_t \times n_t}{(1+r)^i}}{\sum_{i=1}^{L} \frac{E_i}{(1+r)^i}}. \tag{4.6}$$

where CA_f and CA_t are the fixed and turbine dependent components of the Capital Expenditure (CAPEX), defined below. L is the operational lifetime of the array in years, where each year is denoted by i. O_f and O_t are the fixed and turbine dependent components of the Operational Expenditure (OPEX) per year, also defined below. E_i is the energy generated in year i and r is discount rate applied annually.

LCOE uses discounted cash flow analysis to take into account the notion that money has a greater value at present than in the future, with r being the extent to which the value of revenues

and expenditures depreciate each year. New forms of energy are considered risky to investors, so may have a high discount rate, however as tidal energy becomes more established, the discount rate is likely to fall [35]. In this model the simplifying assumption is made that the annual energy generation, E_i, is constant year on year. In practice the yield is likely to vary annually due to the 18.6 year lunar nodal cycle and degradation of the turbine performance for example, however this is not considered at this stage of investigation.

The CAPEX, CA, are the costs incurred in the production and installation of a tidal project. The OPEX, O, are the costs incurred in the maintenance and operation of the array. Both CA and O are split into fixed and turbine-dependent components. The fixed costs are spent regardless of the size of the array, so that the total shared fixed cost per turbine reduces as the number of turbines in the array increases. This economy of volume is a mechanism that has driven down the cost of energy in the wind industry [36]. The turbine costs increase linearly with the number of turbines. For example there may be fixed costs for resource assessments of new sites, establishing a manufacturing centre for turbines, or array to grid connections, but the costs of materials will increase linearly with the number of turbines.

The inputs used for each of these fixed/turbine costs were calculated in previous work by drawing together inputs from multiple sources [35,37–39] and are summarised in Table 7. We consider a range of values for each cost, ranging between pessimistic and optimistic values quoted in literature. We also carry out a Monte Carlo analysis to find the P10, P50 and P90 values of LCOE, by assuming a uniform distribution over each of the cost inputs in Table 7 with the 'pessimistic' and 'optimistic' values as their upper limits to randomly vary between. P10, P50 and P90 are the values for which 10%, 50% and 90% of the LCOE estimates are better (lower) than, respectively. This approach of optimising arrays to minimise LCOE was first presented in [40] for idealised array cases.

Table 7: Estimates for the optimistic (Opt), typical (Typ) and pessimistic (Pes) parameters used in the economic models, and the amount they vary.

Symbol	Description	Value range			Units
		Pes	Typ	Opt	
CA_f	Fixed CAPEX	14.4	9.2	5.6	£m
CA_t	Turbine dependent CAPEX	4.4	3.3	2.4	£m per turbine
O_f	Fixed OPEX	0.87	0.32	0.27	£m per year
O_t	Turbine dependent OPEX	0.26	0.15	0.094	£m per year per turbine
r	Discount rate	0.15	0.10	0.05	N/A
L	Lifetime of an array	20	25	30	years

(b) Results

Figure 4 shows the optimal array designs for the range of break even powers considered. In general, the optimal array layouts span the Alderney Race in fence-like structures orientated perpendicular to the flow direction. This is consistent with findings in [41]. Orientating the turbines in these fence-like structures maximises power generation by preventing the flow from passing around the array as a result of the added turbine drag.

At high levels of break even power, the optimal array contains a low number of turbines in order to mitigate against array blockage effects that detrimentally impact upon power generation. This is synonymous with the early stages of tidal energy development, where the relatively high CAPEX/OPEX and discount rate only permit turbines to be installed in the highest resource areas, otherwise the cost of energy becomes unacceptably high. As the break even power decreases, larger scale arrays become more viable, as it becomes economically acceptable to install turbines in lower energy regions of the Race. It is only once the break even power reduces below

£300/MWh that the array contains turbines in the West Race (i.e. in Alderney territorial waters). This result suggests that to minimise cost of energy, early stage development should take place in French territorial waters, however this may not be the case once different turbine designs (i.e. rotor diameter and rated speed) are considered, as the deeper West Race (Alderney territorial waters) may be more suitable for turbines with a larger rotor diameter, for example.

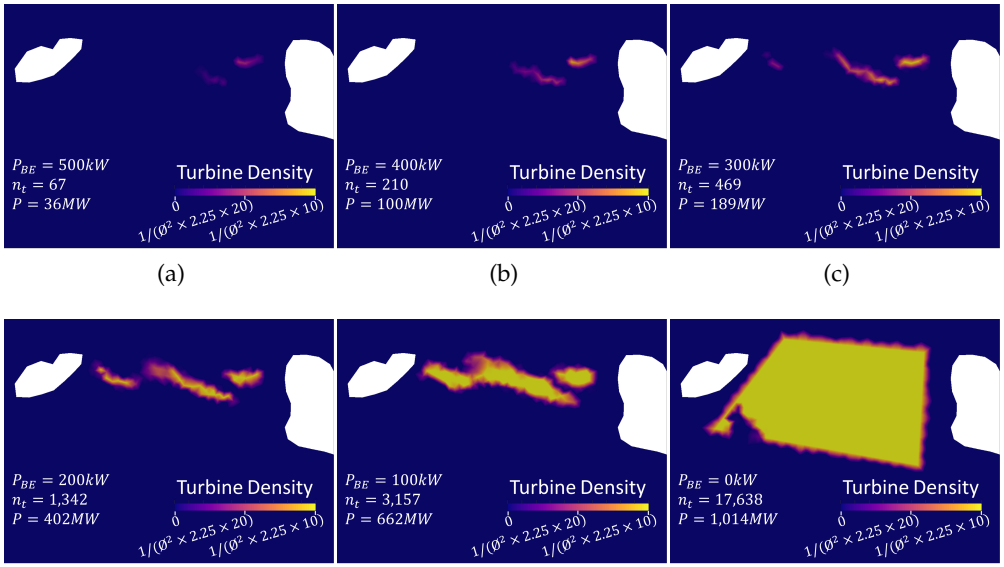

Figure 4: Optimal array design for break even power of (a) 500 kW, (b) 400 kW, (c) 300 kW, (d) 200 kW, (e) 100 kW and (f) 0 kW. The number of turbines and net average power for the optimal array design can be seen for each break even power.

Figure 5 shows the relationship between the break even power and (a) net average array power and corresponding average power per device and (b) number of turbines. Decreasing the break even power reduces the acceptable level of power generation per turbine, so that larger scale arrays become more viable. This has the same impact as reducing CAPEX and/or OPEX, where reductions in CAPEX/OPEX mean that turbines can generate less power to achieve the same LCOE. Mechanisms that enable these CAPEX/OPEX cost reductions include learning taken from previous projects as the industry develops, and cost reduction unlocked by development of the supply chain, for example [32,35]. Economies of volume are inherently modelled as a cost reduction mechanism in this paper through the distinction of the fixed and turbine dependent components of both CAPEX and OPEX. Learning rates as a cost reduction mechanism can be investigated by comparing the impact of moving from the pessimistic to typical to optimal scenarios presented in Table 7.

Increasing the number of turbines increases the total array drag, slowing the flow in the region of the array and thus reducing the available power. When the reduction in CAPEX/OPEX costs achieved from economies of volume outweigh the negative impacts of array blockage, it becomes economically viable to install more turbines. However, the detrimental impacts of array blockage result in a diminishing return on array power as the array size increases. This is illustrated in Figure 6, which shows the relationship between the number of turbines and (a) net average array power, and (b) net average power per device. As the number of turbines increases to very high levels (>2,000 turbines), the net average array power begins to plateau, leveling out to an upper bound of approximately 1 GW by 15,000 turbines.

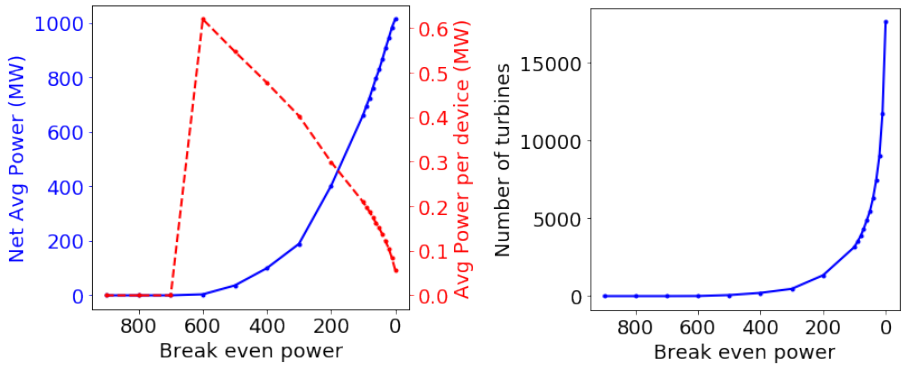

Figure 5: Variation of the macro parameters of the optimal array design with the break even power used in the functional.

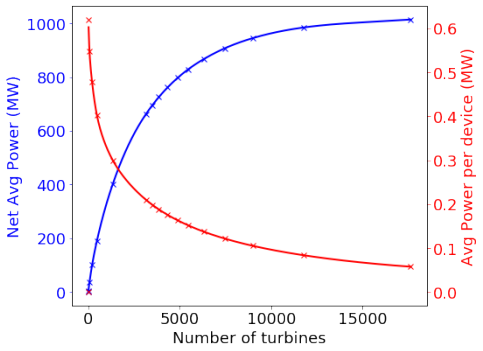

Figure 6: A prediction for the power generated in the optimal array design for all numbers of turbines, achieved by curve fitting between the results of each P_{BE} optimisation.

Figure 7 shows the relationship between the number of turbines in the array and the minimum estimated LCOE. The optimal relationship between number of turbines and LCOE is shown for the 'pessimistic', 'typical' and 'optimistic' scenarios outlined in Table 7, as well as the P10, P50 and P90 estimates obtained from the Monte Carlo analysis. The optimal LCOE estimates are also presented in Table 8. As the number of turbines increases from 0, there is a steep decrease in LCOE, which is enabled through economies of volume. As the number of turbines approaches the optimal value there is a turning point, where the impact of economies of volume vs. diminishing returns from adding more turbines balance out. As the number of turbines increases further the diminishing returns due to blockage have a dominant effect and cause the LCOE to increase. Based on the P50 estimate, a minimum LCOE of £110/MWh is achieved with 38 turbines and an installed capacity of 81 MW. Increasing the installed capacity to 1 GW and 2 GW increases the estimated LCOE to £150/MWh and £180/MWh respectively.

The optimal LCOE obtained from the 'optimistic' and 'pessimistic' cases is £37/MWh and £209/MWh respectively. This disparity between the LCOE estimates is caused as a result of all input parameters being set to their most extreme values. In practice, while there is uncertainty in the associated costs, it is unlikely that all parameters will be at their best or worst at once. This was investigated by estimating the LCOE based on a Monte Carlo analysis, so that a range of CAPEX, OPEX and discount rates could be considered simultaneously. Results in Table 8 show that the P10, P50 and P90 minimum LCOE estimates are £78/MWh, £110/MWh and £146/MWh respectively. Whilst this still provides a broad range, it is significantly reduced in range relative to

the pessimistic and optimistic cases. This disparity in estimated LCOE is likely to reduce further once more cost information becomes available.

Whilst the minimum estimated LCOE can vary widely depending on the cost inputs, the number of turbines required to achieve the minimum LCOE remains largely the same, in the region of 33 to 43 turbines. This is equivalent to a break even power of approximately 550 kW, or a layout with slightly fewer turbines than shown in Figure 4a.

In this work the cost reductions due to learning with time are not explicitly modelled, however the 'pessimistic' scenario would likely correspond to the costs at a very low cumulative installed capacity, and as more arrays are deployed the industry would move towards the increasingly optimistic scenario curves. The further the costs drop, towards the P10 and 'optimistic' scenarios, the flatter the increase in LCOE projection becomes when the number of turbines exceeds the optimal amount to minimise LCOE. The Offshore Renewable Energy Catapult has predicted that learning rates will cause costs to fall by 7% per 100 MW of cumulative deployed capacity [35]. If it is assumed that the 'optimistic' cost inputs can be achieved through learning, as many as 500 turbines, with a total install capacity of 1 GW could be installed whilst still keeping LCOE below £50/MWh.

The typical cost case achieves an optimal LCOE of £110/MWh with 34 turbines. This agrees closely with the P50 estimate, which achieves the same minimum LCOE of £110/MWh with 38 turbines. This estimate falls within 15% of the level of subsidy support proposed by the French government for 'marine hydraulic energy', of £130/MWh (=€150/MWh) [42]. Furthermore, a recent Marine Energy Council report [43] proposed a number of different subsidy schemes to provide a route to market for the tidal energy industry and other innovative clean energy technology types. The typical LCOE predictions are in line with its conclusion that an Innovation Contract for Difference (iCfD) set at an initial level of £150/MWh and falling to £90/MWh could support novel projects in the 5 to 100 MW installed capacity range.

This 'typical' LCOE prediction of £110/MWh falls just below the strike price of £115-120/MWh won by offshore wind farm projects at the Contract for Difference (CfD) auctions in 2014–15 in the UK [44]. Since the time of the 2014–15 CfD auctions in the UK, the LCOE of offshore wind projects in the UK have reduced to around £40/MWh [45], facilitated by the CfD scheme that has enabled economies of volume, economies of scale and technology innovation to drive down costs [35]. This supports the argument that with similar subsidy support, the cost of tidal energy could move from the pessimistic to optimistic levels set out in Table 7.

After 10 MW of installed capacity, the pessimistic LCOE estimate is £295/MWh. The Offshore Renewable Energy Catapult has published figures indicating the LCOE achieved by tidal stream energy was approximately £300/MWh after 10 MW of total installed capacity worldwide (based on 2012 pricing), aligning closely with the pessimistic LCOE approximation in this paper [35]. Likewise this model prediction is in line with the Marine Energy Council report [43] proposal for an Innovation Power Purchase Agreement (IPPA) set at a level of £290/MWh to support novel small-scale projects.

Table 8: Optimal LCOE and corresponding array parameters for different scenarios: optimal, pessimistic and typical scenarios and the P10, P50 and P90 generated using a Monte Carlo based analysis with a uniform distribution and upper and lower limits of the optimistic and pessimistic values.

	Optimistic	Typical	Pessimistic	P10	P50	P90
LCOE (£/MWh)	36.6	109.5	209.0	77.7	110.0	146.2
n_t	42.0	34.0	39.0	46.0	38.0	33.0
P_{avg} (MW)	24.0	19.7	22.4	26.1	21.9	19.2
P_{avg}/n_t (kW)	541	554	546	534	547	556
P_{BE} (kW)	541	554	546	534	547	556

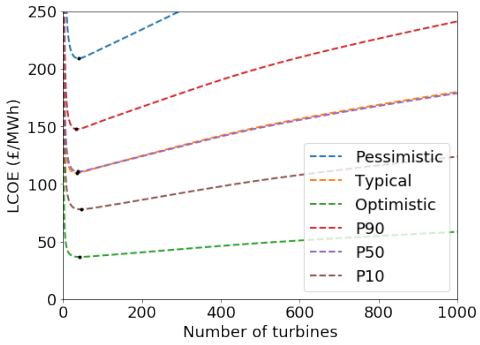

Figure 7: Prediction of optimal LCOE that can be achieved as a function of number of turbines, for the optimistic, pessimistic and typical scenarios outlined in Table 7, and the P10, P50 and P90 values obtained through a Monte Carlo simulation assuming uniform errors.

5. Conclusion

A new, validated *Thetis* model set-up for the English Channel with non-uniform mesh resolution has been used to minimise the LCOE of tidal stream turbine arrays in the Alderney Race. This work considers arrays using turbines with a rated power of 2 MW and a rotor diameter of 16 m. In general, the optimal array solutions consist of 'fence-like structures' of turbines orientated perpendicular to the flow. These array layouts help prevent the flow from diverting around the array as a result of the added array drag and is consistent with previous array optimisation studies [41]. Results demonstrate that in the early stages of array development in the Race (0 – 100 MW of installed capacity), steep reductions in LCOE are achievable through optimisation of turbine placement, and economies of volume. Based on the turbine specification considered in this paper, the optimal location for turbines at this early stage of development is in the East Race.

Given the early stage of tidal stream energy industry development, cost information that provides the inputs to the array optimisation is limited, with a wide range of estimated CAPEX/OPEX and discount rates found in the literature. This uncertainty in associated costs is reflected in the LCOE estimates presented in this work, where the minimum LCOE based on assuming 'pessimistic', 'typical' and 'optimistic' cost scenarios is £36.60/MWh, £109/MWh and £209/MWh respectively. A Monte Carlo analysis is conducted to reflect that it is unlikely that all costs will be at their most extreme (i.e. pessimistic or optimistic) values. Results from this study yield P10, P50 and P90 minimum LCOE estimates of £78/MWh (with 46 turbines), £110/MWh (with 38 turbines) and £146/MWh respectively (with 33 turbines) respectively. This provides a significantly reduced range of LCOE estimates, where the number of turbines required to achieve the minimum LCOE are closely aligned.

There are some notable similarities between the LCOE estimates presented in this work and published data from industry. For example, in this paper, the pessimistic LCOE estimate after 10 MW of installed capacity (i.e. when economies of volume are limited) is £295/MWh. This aligns closely with information published by the Offshore Renewable Energy Catapult, who estimate that the LCOE after 10 MW of installed capacity worldwide was £300/MWh, based on 2012 prices and aggregated data from multiple tidal stream turbine developers.

Additional cost reduction mechanisms such as learning rates are not considered explicitly in this work. However, it could be argued that learning will allow costs to drop from the more pessimistic end towards the optimistic levels found in the literature. If this is possible, it is estimated that a 1 GW array could achieve an LCOE of £49/MWh, based on optimistic cost inputs.

6. Limitations and further work

Aspects of the work presented in this paper can be developed further to reduce uncertainty in the results. This includes improvement to model validation in order to reduce error in modelled velocities, owing in part to the coarseness of the mesh required to provide acceptable run times when using the model within an optimisation loop. This can translate into large errors in power. At the settings used in this model the mean velocity is generally underestimated, so it is likely that the conclusions are conservative relative to what can be achieved in reality. However wave effects, which have been shown to lead to a net reduction in tidal power, have not yet been included in this work. Since wave effects can have a notable impact, especially in sites more exposed to waves, they should be included in future studies [10,11].

Another area of further work is consideration for a suitable range of turbine scales for the Alderney Race. The current work considers 16m rotors only, however it has been shown that LCOE could reduce significantly if turbine diameter is increased, even by a few metres [32]. It will be important in future array optimisation work to identify the rotor diameter limits within different regions of the Race to establish how best to harness the resource with different turbine sizes. This also requires an understanding of any constraints that would prevent turbines from being installed in specific regions of the Alderney Race. For example, local areas with uneven bathymetry may prevent turbines from being installed [46].

The impacts of local blockage and accelerated bypass flow on the yield of tidal stream turbines in large-scale arrays should also be considered [47]. Given that resolving turbines individually requires a much finer mesh and is computationally very expensive, a number of approaches would need to be investigated. A two stage optimisation as described in [2] could be implemented, such that continuous optimisation provides a good initial layout, so that the discrete turbine micro-siting optimisation requires overall fewer costly iterations to converge.

The LCOE calculations should be updated once additional cost information becomes available. Additional cost information will also be important to validate the assumptions made in this paper, such as the linear increase in OPEX with number of turbines, for example.

Authors' Contributions. ZLG carried out the numerical modelling, with assistance from DSC on the setup and validation. MDP and DSC provided supervision throughout. All authors read and approved the manuscript.

Competing Interests. The authors declare that they have no competing interests.

Funding. ZLG acknowledges the support of an EPSRC PhD studentship, through the Mathematics of Planet Earth CDT and the support of the National Productivity Investment Fund through NERC and the Grantham Institute. DSC acknowledges the support of the International Centre for Infrastructure Futures (ICIF) under grant EP/K012347/1. MDP acknowledges the support of EPSRC under grants EP/M011054/1 and EP/R029423/1.

References

1. D. S. Coles, L. S. Blunden, and A. S. Bahaj, "Assessment of the energy extraction potential at tidal sites around the Channel Islands," *Energy*, 2017.
2. S. W. Funke, S. C. Kramer, and M. D. Piggott, "Design optimisation and resource assessment for tidal-stream renewable energy farms using a new continuous turbine approach," *Renewable Energy*, 2016.
3. D. S. Coles, L. S. Blunden, and A. S. Bahaj, "The energy yield potential of a large tidal stream turbine array in the Alderney Race," *Philosophical Transactions A*, 2020.
4. T. Kärnä, B. de Brye, O. Gourgue, J. Lambrechts, R. Comblen, V. Legat, and E. Deleersnijder, "A fully implicit wetting-drying method for DG-FEM shallow water models, with an application to the Scheldt Estuary," *Computer Methods in Applied Mechanics and Engineering*, no. 5-8, 2011.
5. C. V. M. Vouriot, A. Angeloudis, S. C. Kramer, and M. D. Piggott, "Fate of large-scale vortices in idealized tidal lagoons," *Environmental Fluid Mechanics*, 2019.
6. F. Rathgeber, D. A. Ham, L. Mitchell, M. Lange, F. Luporini, A. T. McRae, G. T. Bercea, G. R. Markall, and P. H. Kelly, "Firedrake: Automating the finite element method by composing abstractions," *ACM Transactions on Mathematical Software*, no. 3, 2016.

7. T. Kärnä, S. C. Kramer, L. Mitchell, D. A. Ham, M. D. Piggott, and A. M. Baptista, "Thetis coastal ocean model: discontinuous Galerkin discretization for the three-dimensional hydrostatic equations," *Geosci. Model Dev*, vol. 11, pp. 4359–4382, 2018.
8. W. Pan, S. C. Kramer, and M. D. Piggott, "Multi-layer non-hydrostatic free surface modelling using the discontinuous Galerkin method," *Ocean Modelling*, 2019.
9. G. D. Egbert, S. Y. Erofeeva, and R. D. Ray, "Assimilation of altimetry data for nonlinear shallow-water tides: Quarter-diurnal tides of the Northwest European Shelf," *Continental Shelf Research*, no. 6, 2010.
10. M. J. Lewis, S. P. Neill, M. R. Hashemi, and M. Reza, "Realistic wave conditions and their influence on quantifying the tidal stream energy resource," *Applied Energy*, 2014.
11. M. R. Hashemi, S. P. Neill, P. E. Robins, A. G. Davies, and M. J. Lewis, "Effect of waves on the tidal energy resource at a planned tidal stream array," *Renewable Energy*, 2015.
12. J. Thiébot, P. Bailly du Bois, and S. Guillou, "Numerical modeling of the effect of tidal stream turbines on the hydrodynamics and the sediment transport - Application to the Alderney Race (Raz Blanchard), France," *Renewable Energy*, 2015.
13. S. Draper, T. A. Adcock, A. G. Borthwick, and G. T. Houlsby, "Estimate of the tidal stream power resource of the Pentland Firth," *Renewable Energy*, 2014.
14. R. A. Walters, M. R. Tarbotton, and C. E. Hiles, "Estimation of tidal power potential," *Renewable Energy*, vol. 51, pp. 255–262, 3 2013.
15. R. H. Karsten, J. M. Mcmillan, M. J. Lickley, and R. D. Haynes, "Assessment of tidal current energy in the Minas Passage, Bay of Fundy," vol. 222, no. 5, pp. 493–507, 2008.
16. N. O. Centre, "Harmonic constituents at several gauge locations," Personal Communication with J. Eric Jones., 2011.
17. Edina Digimap Service, "Hydrospatial one, gridded bathymetry," http://digimap.edina.ac.uk/marine/, 2014, , SeaZone Solutions Ltd, Online; accessed 2017.
18. D. C. Kapoor, "General bathymetric chart of the oceans (gebco)," *Marine Geodesy*, vol. 5, no. 1, pp. 73–80, 1981. [Online]. Available: https://doi.org/10.1080/15210608109379408
19. P. Wessel and W. H. F. Smith, "A global, self-consistent, hierarchical, high-resolution shoreline database," *Journal of Geophysical Research: Solid Earth*, no. B4, 1996.
20. Z. Goss, S. Warder, A. Angeloudis, S. C. Kramer, A. Avdis, and M. D. Piggott, "Tidal modelling with Thetis: preliminary English Channel benchmarking," Imperial College, Tech. Rep., 2019.
21. T. A. A. Adcock, S. Draper, G. T. Houlsby, A. G. L. Borthwick, and S. Serhadlıoğlu, "The available power from tidal stream turbines in the Pentland Firth."
22. "Bed roughness and friction factors in estuaries - MarineSpecies Introduced Traits Wiki." [Online]. Available: http://www.marinespecies.org/introduced/wiki/Bed_roughness_and_friction_factors_in_estuaries#Manning-Strickler_formula
23. C. I. Willmott, "On the validation of models," Tech. Rep. 2, 1981.
24. J. Thiébot, N. Guillou, S. Guillou, A. Good, and M. Lewis, "Wake field study of tidal turbines under realistic flow conditions," *Renewable Energy*, vol. 151, pp. 1196–1208, 5 2020.
25. N. Guillou, G. Chapalain, and S. P. Neill, "The influence of waves on the tidal kinetic energy resource at a tidal stream energy site," *Applied Energy*, vol. 180, pp. 402–415, 2016. [Online]. Available: https://hal.archives-ouvertes.fr/hal-01672290
26. A. Sentchev and C. Author, "Underway velocity measurements in Alderney Race: toward a three-dimensional representation of tidal motions," *Philosophical Transactions A*, 2020. [Online]. Available: http://dx.doi.org/10.1098/rsta.2019.0491
27. "Bathymetric DTM Atlantic facade (Homonim Project)," SHOM, Tech. Rep., 2015.
28. S. W. Funke, P. E. Farrell, and M. D. Piggott, "Tidal turbine array optimisation using the adjoint approach," *Renewable Energy*, 2014.
29. C. Legrand, "Assessment of Tidal Energy Resource," EMEC, Tech. Rep., 2009. [Online]. Available: http://www.emec.org.uk/assessment-of-tidal-energy-resource/
30. "Bluemull Sound." [Online]. Available: https://www.novainnovation.com/bluemull-sound
31. "Lessons Learnt from MeyGen Phase 1A Part 2/3: Construction Phase," Meygen Ltd, Tech. Rep., 2018. [Online]. Available: https://s3-eu-west-1.amazonaws.com/media.newore.catapult/app/uploads/2018/06/05103702/Lessons-Learnt-from-MeyGen-Phase-1a-Part-2-of-3-Design-Phase.pdf
32. D. S. Coles and T. Walsh, "Mechanisms for reducing the cost of tidal stream energy," in *EWTEC 2019*, no. 1836, 2019.
33. "SIMEC Atlantis Energy Unveils World's Largest Single Rotor Tidal Turbine, the AR2000 | SIMEC Atlantis Energy." [Online]. Available: https://simecatlantis.com/2018/09/13/simec-atlantis-energy-unveils-worlds-largest-single-rotor-tidal-turbine-the-ar2000/

34. A. S. Bahaj, A. F. Molland, J. R. Chaplin, and W. M. J. Batten, "Power and thrust measurements of marine current turbines under various hydrodynamic flow conditions in a cavitation tunnel and a towing tank," *Renewable Energy*, no. 3, 2007.
35. G. Smart and M. Noonan, "Tidal stream and wave energy cost reduction and industrial benefit, Summary Analysis," Catapult Offshore Renewable Energy, Tech. Rep., 2018.
36. P. Higgins and A. M. Foley, "Review of offshore wind power development in the United Kingdom," in *2013 12th International Conference on Environment and Electrical Engineering*, 2013.
37. "International levelised cost of energy for ocean energy technologies," IEA Technology Collaboration Programme for Ocean Energy Systems (OES), Tech. Rep., 2015. [Online]. Available: https://www.ocean-energy-systems.org/news/international-lcoe-for-ocean-energy-technology/
38. Hamilton, Mark, "Technology Update," Scotrenewables Tidal Power Ltd, Tech. Rep., 2012.
39. "Cost of and financial support for wave, tidal stream and tidal range generation in the UK Executive summary Background," Ernst & Young LLP, Tech. Rep., 2010.
40. Z. L. Goss, D. S. Coles, S. C. Kramer, and M. D. Piggott, "Efficient optimisation of economic functionals in large-scale tidal stream arrays," *In preparation*, 2020.
41. D. Coles, S. C. Kramer, M. D. Piggott, A. Avdis, and A. Angeloudis, "Optimisation of tidal stream turbine arrays within Alderney Race," in *EWTEC 2017*, pp. 1–10.
42. I. Renewable Energy Agency, "Tidal Energy Technology Brief," Tech. Rep., 2014. [Online]. Available: www.irena.org
43. "UK Marine Energy 2019 - A new industry," Tech. Rep., 2019.
44. "Contracts for Difference (CFD) Allocation Round One Outcome," Department of Energy and Climate Change, Tech. Rep.
45. "Contracts for Difference Allocation Round 3 Results," Department for Business, Energy and Industrial Strategy, Tech. Rep., 2019.
46. T. Schwedes, D. A. Ham, S. W. Funke, and M. D. Piggott, *Mesh Dependence in PDE-Constrained Optimisation*. Springer International Publishing, 2017.
47. C. A. Consul, R. H. Willden, and S. C. McIntosh, "Blockage effects on the hydrodynamic performance of a marine cross-flow turbine," *Philosophical Transactions of the Royal Society A: Mathematical, Physical and Engineering Sciences*, no. 1985, 2013.